Met. Mater. Int., Vol. 23, No. 5 (2017), pp. 877~883
doi: 10.1007/s12540-017-7089-7

Effect of Ti Content on Creep Properties of Ni-Base Single Crystal Superalloys

Baig Gyu Choi[1,*], In Soo Kim[1], Hyun Uk Hong[2], Jeonghyeon Do[1], Joong Eun Jung[1], and Chang Yong Jo[1]

[1]High Temperature Materials Department, Korea Institute of Materials Science, Changwon 51508, Republic of Korea
[2]Department of Materials Science and Engineering, Changwon National University, Changwon 51140, Republic of Korea

(received date: 2 February 2017 / accepted date: 25 April 2017)

The effect of Ti content on the creep properties and microstructures of experimental Ni-base single crystal superalloys has been investigated. The experimental alloys were designed to provide better high temperature properties than the commercial single crystal alloy CMSX-4. The creep properties of the experimental alloys, Alloy 2 and Alloy 3, were superior to those of CMSX-4. Alloy 3 showed a longer creep life than Alloy 2 at 900 °C and 950 °C, while it has similar creep life with Alloy 2 at 982 °C. Transmission electron microscopy micrographs of the experimental alloys after the creep test showed distinct deformation features as a function of temperature and Ti content. The dissociation of dislocations into partial dislocations with stacking faults in Alloy 3 was found to improve resistance to creep deformation at 950 °C. The effect of Ti on the creep deformation mechanism was not evident at 982 °C, which resulted in similar creep properties in both experimental alloys. The transition of the γ′ cutting mechanism from dislocations coupled with stacking faults to anti-phase boundary coupled pairs occurred both in Alloy 2 and Alloy 3. However, the transition temperature was higher in Alloy 3 than in Alloy 2 because of the difference in Ti contents.

Keywords: alloys, Ni-based superalloy, casting, creep, transmission electron microscopy (TEM)

1. INTRODUCTION

Ni-base single crystal superalloys are widely used as blade materials for gas turbines because of their excellent high temperature performance [1,2]. Since single crystal superalloys were first used for blades in jet engines in the 1970s, many single crystal superalloys have been developed to enhance the temperature capability [3,4]. The generation of single crystal superalloys is classified according to the alloy composition, especially the contents of Re, Ru, and other platinum group elements. Generally, higher generation alloy, which contain higher amounts of Re and/or Ru, exhibit better high temperature performance [5]. However, the second generation single crystal superalloys with 3% Re have been applied to real engines more preferentially than advanced generation alloys because they provide a reasonable balance between properties and price.

Experimental single crystal superalloys with 3% Re have been designed to have good high temperature performance. On the basis of the effects of alloying elements on the microstructure and mechanical properties, various compositions have been considered as candidates of the base alloy. Two derivatives of the base alloy, Alloy 2 and Alloy 3, were selected because of their good high temperature properties. These two alloys had much better creep resistance than the commercial single crystal superalloy, CMSX-4 under various creep conditions, as shown in Table 1.

The difference between Alloy 2 and Alloy 3 was in the amount of γ′ forming elements. It is generally known that the mechanical properties of superalloys are greatly influenced by their γ′ phase characteristics, which is the major strengthening phase of superalloys. The creep properties of single crystal superalloys are affected by the volume fraction of γ′ [6], the lattice misfit between γ and γ′ [4,7,8], planar fault energies such as stacking fault energy (SFE) [9] and anti-phase boundary energy (APBE) [10], all of which depend on the composition. Ti is a constitutive element of the γ′ phase and it substitutes Al atoms in γ′, Ni_3Al [11]. The γ/γ′ misfit is affected by the amount of Ti added because the lattice parameter of γ′ increases with increasing Ti amount [12]. APBE and SFE also increase with increasing Ti amount [13,14], which affects the shearing

Table 1. Creep rupture lives in hours of CMSX-4 and experimental alloys under various conditions

Alloys	900 °C/500 MPa	950 °C/355 MPa	982 °C/248 MPa
CMSX-4	144	123	231
Alloy2	177	212	379
Alloy3	281	302	408

*Corresponding author: choibg@kims.re.kr

mechanisms that are active in superalloys at elevated temperatures.

The only difference in chemical composition between Alloy 2 and Alloy3 is the amount of γ′ forming elements while obviously distinct creep behaviors were obtained at and below 950 °C. In this study, the detailed mechanisms in creep deformation of the two alloys were investigated in relation to the dislocation structures after creep deformation as well as to the required the energies for anti-phase boundary and stacking fault formation.

2. EXPERIMENTAL PROCEDURE

The chemical compositions of the experimental alloys and CMSX-4 are shown in Table 2. The experimental alloys had more refractory elements such as W and Mo which enhanced the creep properties because of their solid solution hardening effects on the alloys. Ru (1%) was also added to restrain topologically close-packed (TCP) phase formation and to increase the negative γ/γ′ lattice misfit which is known to enhance the creep strength [7,8]. The amounts of Cr in the experimental alloys, which also enhances thermal stability and restrain TCP phase formation, were less than that in CMSX-4. The composition of the γ′-forming elements in Alloy 2, Al and Ti, were modified in Alloy 3 to enhance the strengthening effect of γ′.

Master ingots of the experimental alloys were made in a vacuum induction melting furnace. The master ingots were remelted, and cast into single crystal rods 13 mm in diameter by the Bridgman method. The growth directions of all the single crystal rods had angular deviations from the [001] crystallographic direction within 10°. Therefore, the variation of creep properties owing to anisotropy was not significant. The single crystal rods were subjected to solutionizing followed by double aging according to optimized temperature cycles selected from among various candidate heat treatment conditions on the basis of microstructural observation. The solutionizing temperature was 1315 °C for both alloys. Double aging for Alloy 2 and Alloy 3 was carried out at 1140 °C and 871 °C respectively. A series of creep tests under 900 °C/500 MPa, 950 °C/355 MPa, and 982 °C/248 MPa conditions were conducted to verify the properties of the experimental alloys. The tensile creep loading direction was the same as the growth direction of each single crystal. Scanning electron microscopy (SEM) and transmission electron microscopy (TEM) on the aged and the crept states of the experimental alloys were carried out. After creep tests, the specimens were cut parallel to the tensile loading axis. The specimens for SEM observation were prepared by mechanical polishing followed by chemical etching. The specimen was dipped into Kallings' II reagent for a few seconds to reveal γ′ in the SEM images. TEM foils were electrochemically polished with a twin jet polisher using a solution of 10% perchloric acid in ethanol at the applied voltage and temperature of 20 V and -30 °C, respectively.

3. RESULTS AND DISCUSSION

3.1. Initial microstructure of the alloys

The γ′ morphology of the plane perpendicular to the growth direction of the single crystal was observed with STEM as shown in Fig. 1. The heat treated experimental alloys had similar microstructures of uniformly distributed γ′ precipitates in

Table 2. Chemical composition of CMSX-4 and experimental alloys (in wt%)

Alloy	Ni	Co	Cr	Al	Ti	Ta	Mo	W	Re	Ru	Hf
CMSX-4	Bal.	9	6.4	5.6	1	6.5	0.6	6.4	3	0	0.1
Alloy2	Bal.	11.5	4	5.5	1	7	1	8	3	1	0
Alloy3	Bal.	11.5	4	4.5	3	7	1	8	3	1	0

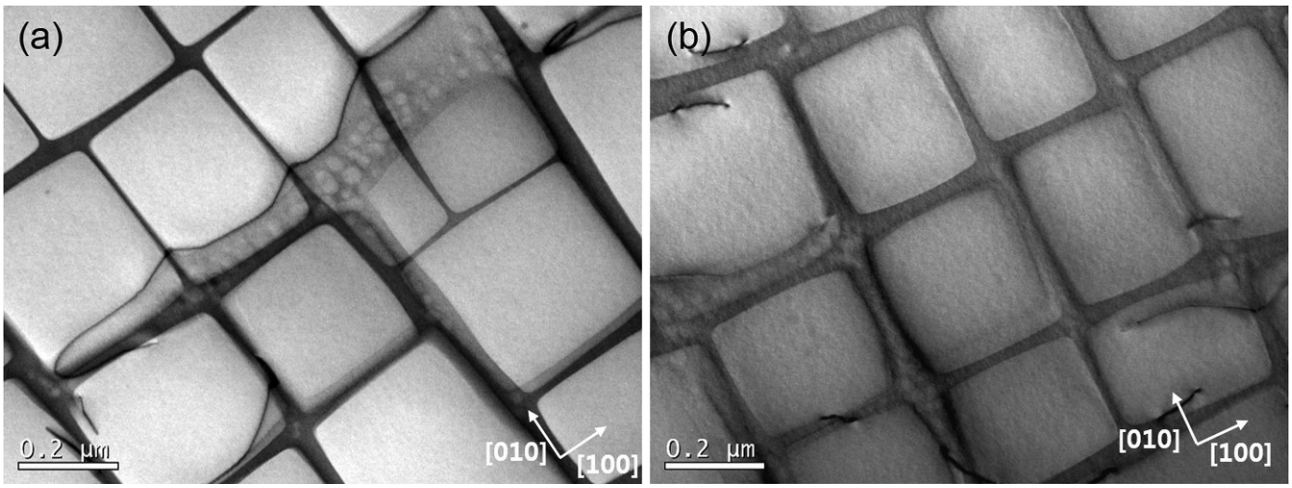

Fig. 1. STEM images showing γ′ morphology after heat treatments; (a) Alloy 2 and (b) Alloy 3.

a γ matrix. The cuboidal γ′ particles of the two experimental alloys were only slightly different in size, and thus γ′ size had a negligible effect on high temperature creep properties. Small spherical secondary γ′ were observed within the γ channel in both alloys, especially where there was a wide gap between γ′ cuboids. A few interfacial dislocations were found at the interface between γ and γ′.

It is well known that the γ/γ′ lattice misfit strongly influences the morphology and size of coherent precipitates, γ′ in single crystal superalloys, as well as their high temperature properties [15]. When the lattice misfit is small, interfacial energy becomes the dominant factor and spherical γ′ form to minimize their surface area with the same volume. As the lattice misfit increases, the elastic strain energy induced by lattice misfit is dominant and cuboidal γ′ particles precipitate [15].

The γ/γ′ lattice misfit, δ, is defined as $\delta = 2(a_{\gamma'} - a_{\gamma})/(a_{\gamma'} + a_{\gamma})$ where a_{γ} and $a_{\gamma'}$ are the lattice parameters of γ and γ′, respectively. In this study, the γ/γ′ lattice misfit was calculated by the commercial software, JMatPro with the TTNi8 database made by ThermoTech. The calculated γ/γ′ lattice misfits at the first aging temperature, 1140 °C, were -0.335% and -0.382% for Alloy 2 and Alloy 3, respectively. The difference of lattice misfit, however, is not enough to generate a morphological change of γ′ between the two alloys, as already shown in Fig. 1.

3.2. Creep at 900 °C/500 MPa

The creep curves of experimental alloys at 900 °C/500 MPa are displayed in Fig. 2. Alloy 3 shows much better creep resistance than Alloy 2. TEM micrographs of the alloys after the creep tests, shown in Fig. 3, show very different dislocation arrays between the two alloys. In Alloy 2, a large number of dislocations are shearing γ′, which seems to be predominantly responsible for the deformation. The density of superdislocations in the γ′ phase of Alloy 2 after the creep test is higher than that of Alloy 3, as shown in Fig. 3(a) and (b). A few SFs were observed in the γ′ of Alloy 2, whereas more SFs and fewer

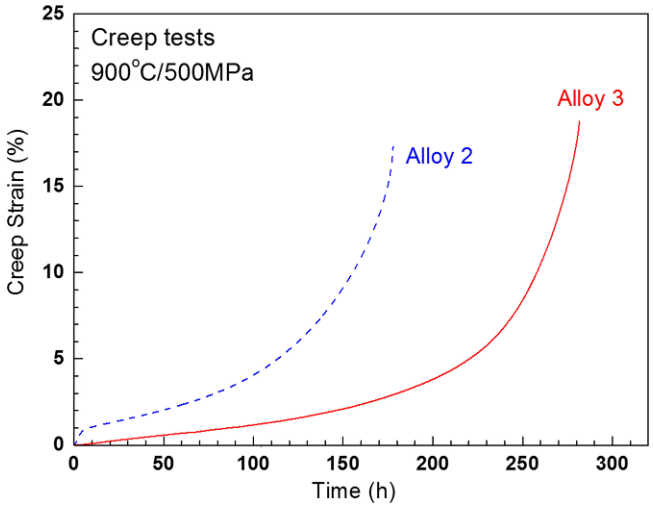

Fig. 2. Creep curves at 900 °C/500 MPa.

dissociated superdislocations with APB were found in the γ′ of Alloy 3. Even though the planar defects in Fig. 3(b) are not striped, they can be identified as SFs, like SFs without stripes in previous reports [16,17]. Several straight lines indicated with arrows are observed in Fig. 3(b), which were identified as SFs on other octahedral planes under another beam direction. The creep deformation of Alloy 3 therefore seems to be attributed by SF formation.

In a γ/γ′ two phase alloy, deformation begins in the matrix [18]. Further deformation causes the dislocation to cut through γ′ particles at the stress concentrated region. It is well known that a<110> superdislocation may dissociate by various mechanisms which could produce APB, complex stacking faults (CSFs), superlattice extrinsic stacking faults (SESFs), or superlattice intrinsic stacking faults (SISFs) [19,20].

By considering the compositional difference between the two alloys, it can be inferred that a relatively high amount of Ti induced well-developed SFs in Alloy 3 owing to varia-

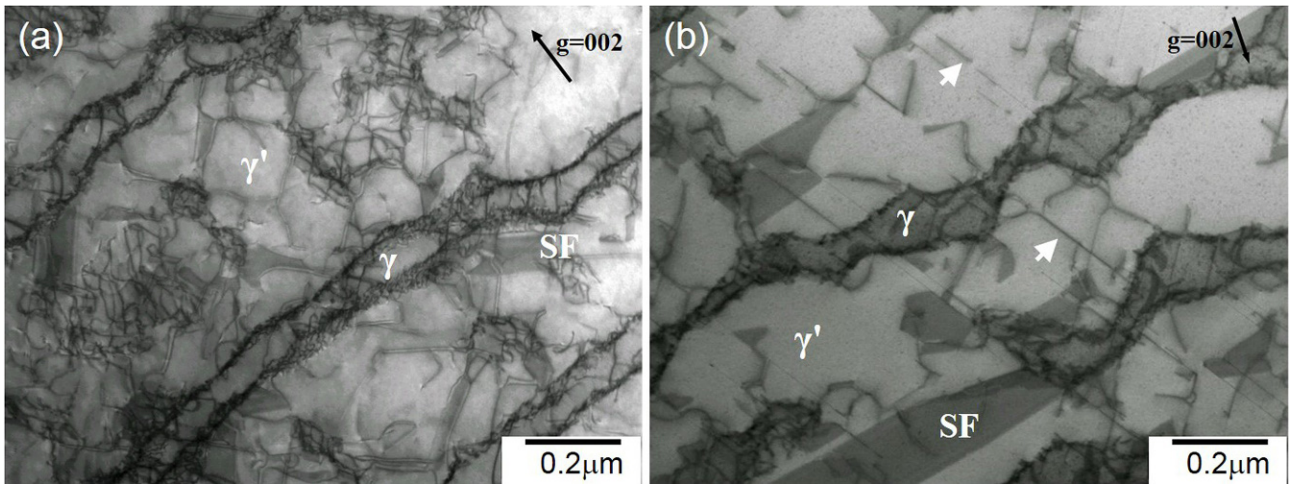

Fig. 3. TEM micrographs showing microstructures after creep tests at 900 °C/500 MPa of (a) Alloy 2 and (b) Alloy 3. B = close to [110].

tions in the SFE. It was reported that Ti significantly increases the SFE of γ′, Ni_3Al [13]. More Ti in Ni_3Al would hinder the formation of SF in γ′. However, this conflicts with the results of the TEM observation shown in Fig. 3, in which more SFs were observed in Alloy 3. Not only may the SFE increase but also the variation of the APBE may have a strong effect on the dissociation of dislocations, as well as on the manner of shearing through γ′ particles. The required energy for APB formation is also dependent on Ti content; APBE also increases when Ti is added into Ni_3Al [14]. Increasing APBE causes APB coupled pairs to be unfavorable for the shearing of γ′.

The effect of Ti on the increase of SFE seems to be less dominant than that on the increase of APBE in the experimental alloys because more SFs were found in Alloy 3 after the creep test. Dislocation mobility could be reduced by the dissociation of dislocations with SF in the γ′ phase. Low dislocation mobility owing to higher Ti content increases the resistance to creep deformation of Alloy 3.

3.3. Creep at 950 °C/355 MPa

The creep curves of the alloys at 950 °C/355 MPa are shown in Fig. 4. The creep life of Alloy 3 was longer than that of Alloy 2 under these conditions. SEM micrographs after creep tests at 950 °C/355 MPa revealed well-developed rafted structures in both alloys, as shown in Fig. 5. There is no significant difference between the two alloys.

Figure 6 shows the TEM micrographs of the specimens under 950 °C/355 MPa after creep tests. Some superdislocation debris, which indicates the interactions of super partial dislocations, are observed in Alloy 2, indicated by the arrows. A fairly long SF within the γ′ phase could be observed in Alloy 3 [Fig. 6(b)] whereas no SF was found in Alloy 2 after creep. The results reveal that there are considerable differences in the dislocation structure of Alloy 2, in contrast to several SFs within the γ′ after creep at a lower temperature, 900 °C.

SFE is known to be dependent upon temperature [21,22].

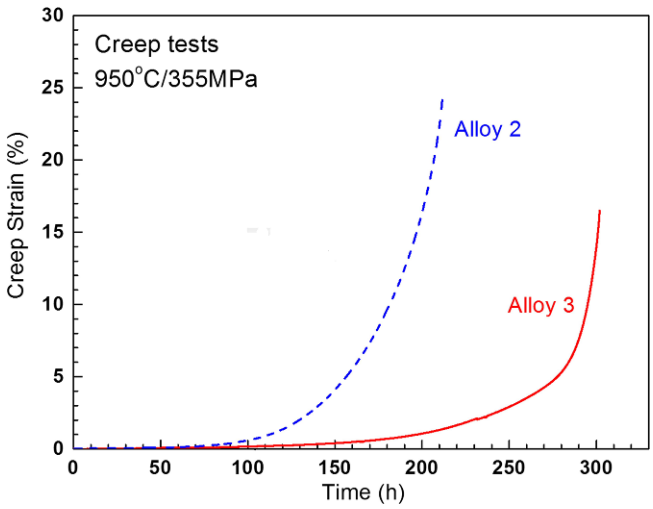

Fig. 4. Creep curves at 950 °C/355 MPa.

Remy *et al*. [21] previously found that SFE increased with temperature in most of the face centered cubic (FCC) systems of their study. Tian *et al.* [22] also reported that SFE of the γ′ phase increased in the 760 °C and 1070 °C temperature range in single crystal superalloys. In the present study, SF formation in Alloy 2 became more difficult under the 950 °C/355 MPa condition than under the 900 °C/500 MPa condition because of the higher SFE. In the case of Alloy 3, shearing of the γ′ particles by dislocations coupled with SF still occurred even at 950 °C. The dissociation of dislocations into partial dislocations with SF resulted in the significantly longer creep life of Alloy 3 than Alloy 2.

Kruml *et al.* [23] reported that APBE of a γ′ compound ($(Ni_{74.8}Al_{21.9}Hf_{3.3})$ decreased slowly with increasing temperature, whereas Wang *et al.* [14] showed that the required energy for APB formation on the (111) plane of a γ′ compound with Ti reached a maximum value near 1327 °C. APBE of the present alloys can be considered to increase with increasing tem-

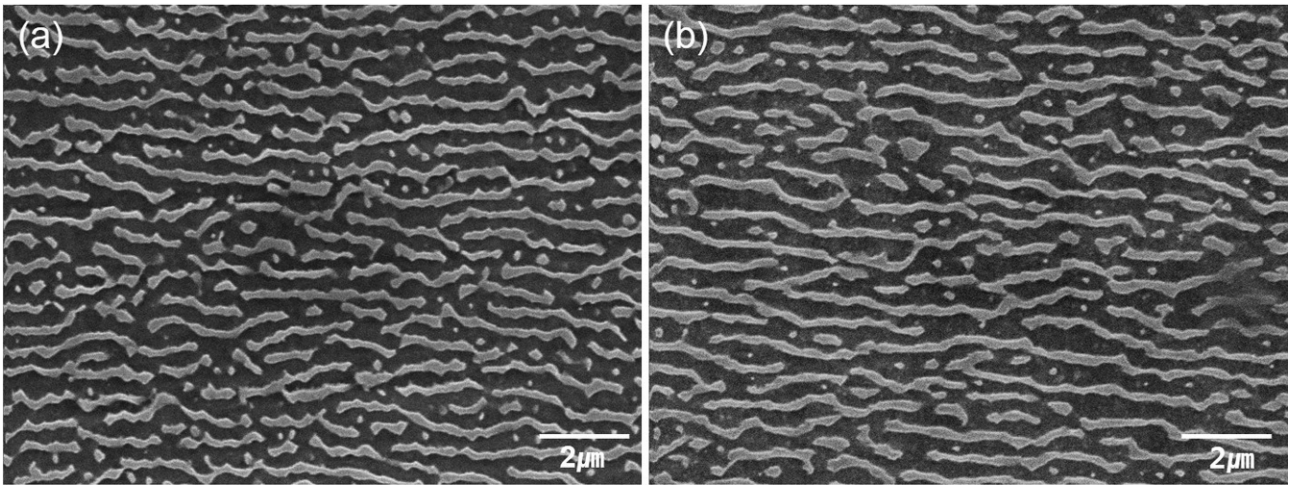

Fig. 5. SEM micrographs showing rafted γ′ after creep tests at 950 °C/355 MPa of (a) Alloy 2 and (b) Alloy 3.

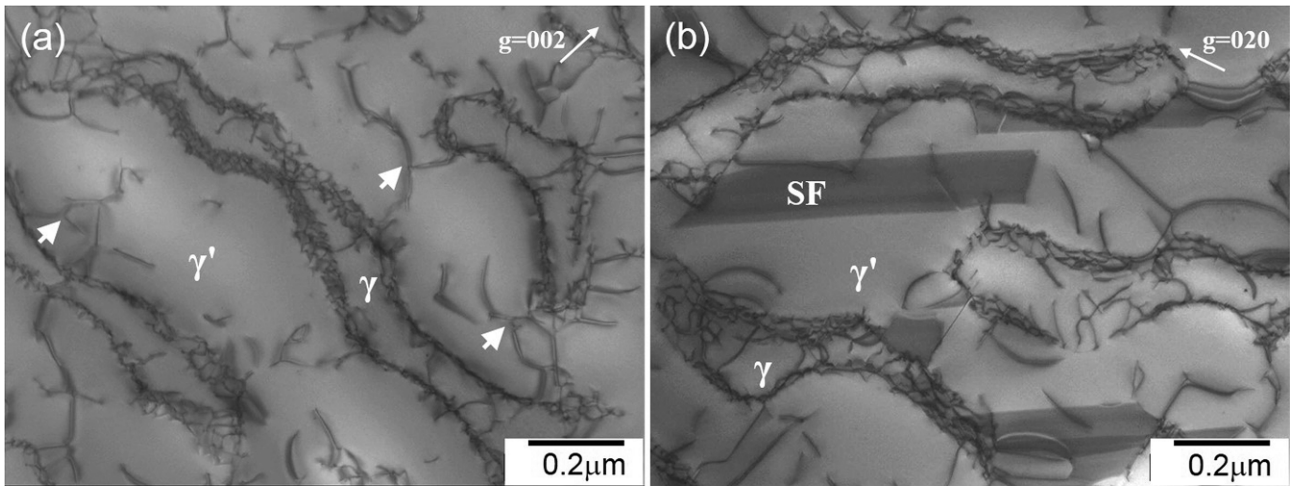

Fig. 6. TEM micrographs showing microstructures after creep tests at 950 °C/355 MPa of (a) Alloy 2 with B = close to [100] and (b) Alloy 3 with B = close to [101].

perature, as suggested by Wang *et al.* [14], within the creep temperature range because Kruml *et al.* [23] discussed the APBE of a γ′ compound with Hf whereas Wang *et al.* [14] discussed Ni-Al-Ti system similar that used in the current study.

Although the temperature dependence of APBE with alloy compositions including sign and magnitude is still disputable, the increase of SFE with increasing temperature is more remarkable than that of APBE in the current alloys because cutting γ′ of superdislocations with APB is dominant at higher temperature in Alloy 2.

3.4. Creep at 982 °C/248 MPa

Figure 7 shows the creep curves of the two alloys under 982 °C/248 MPa conditions, describing similar response to creep behavior as compared to lower temperature tests. The deformed microstructure observed by STEM is shown in Fig. 8. Dislocation networks on the rafted γ/γ′ interface clearly developed in Alloy 2 and Alloy 3. Interfacial dislocation networks are generally formed by dislocation reactions between the misfit dislocations caused by the difference in lattice parameter between γ and γ′; these dislocations generate owing to stress during the creep tests [8]. At higher temperatures, climb of dislocations, which is a thermally activated process, becomes favorable. There is enough energy to arrange dislocations caused by glide and climb at the γ/γ′ interface, which enables the development of dislocation networks [24]. A dislocation network in the interface hinders the partial dislocation which can be dissociated with SF or APB from entering γ′ precipitates. Matrix dislocations pile up at the interfaces, which generates sufficient local stresses for cutting of the γ′ phase. It is known that fine dislocation networks owing to more negative misfit enhance the creep properties [4]. The γ/γ′ lattice misfit at the creep temperature was also calculated by JMatPro using a heat treatment temperature of 982 °C. The values were -0.055% and -0.047% for Alloy 2 and Alloy 3, respectively. Generally the lattice misfit of a superalloy depends on not only composition but also temperature because of the difference in the thermal expansion coefficient of γ and γ′ [25]. The difference in lattice mismatch between Alloy 2 and Alloy 3 decreased more at 982 °C than at the first aging temperature, and this difference did not make a significant difference in the dislocation networks as shown in Fig. 8.

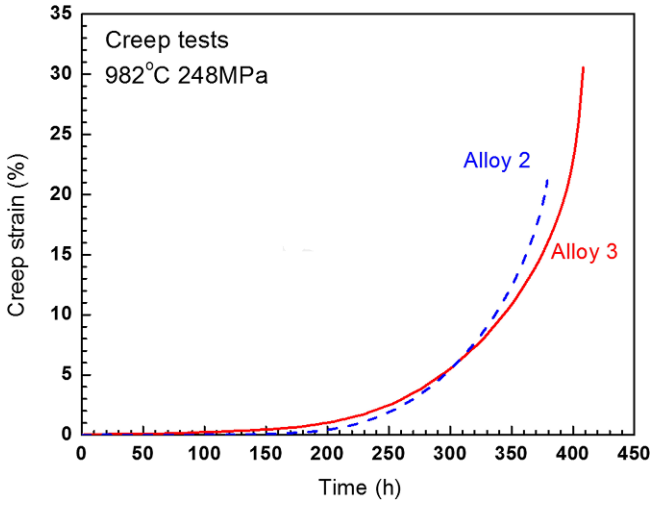

Fig. 7. Creep curves at 982 °C/248 MPa.

The pair of superdislocations coupled with APB cutting into the γ′ precipitates are observed in Figs. 8(a) and 8(b), where only a few stacking faults are visible in Alloy 3. At 950 °C, the greatest difference in the dislocation structure after creep tests between Alloy 2 and Alloy 3 was the SFs in the γ′ phase. However, SF shearing did not contribute to the creep deformation mechanism of the alloys, even in Alloy 3 whose creep deformation was mainly governed by SF shearing at and below 950 °C.

As previously discussed, the increases of SFE with increas-

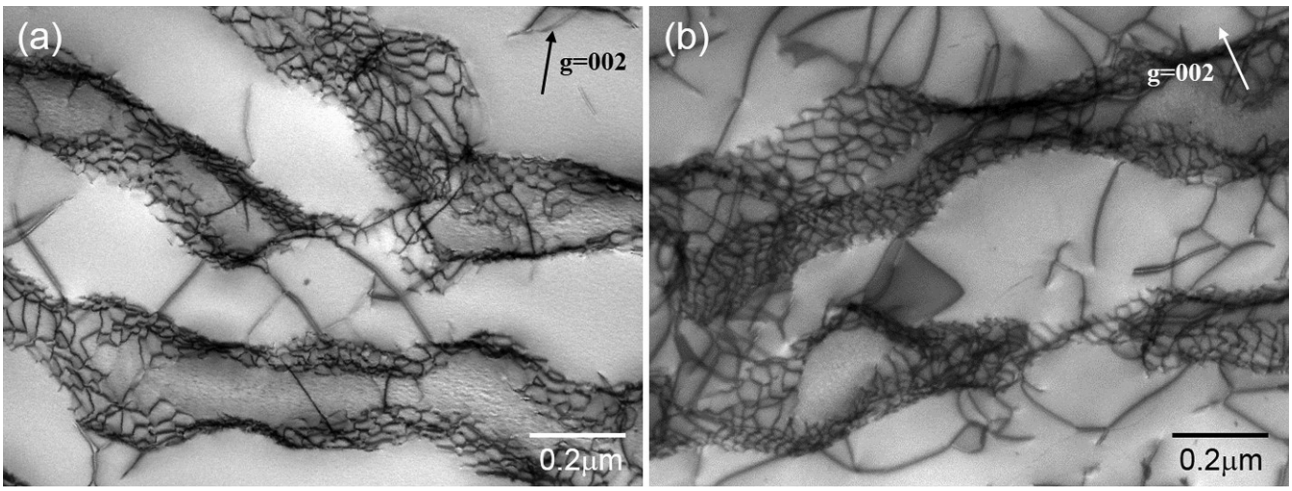

Fig. 8. STEM micrographs showing microstructures after creep tests at 982 °C/248 MPa of (a) Alloy 2 and (b) Alloy 3. B = close to [100].

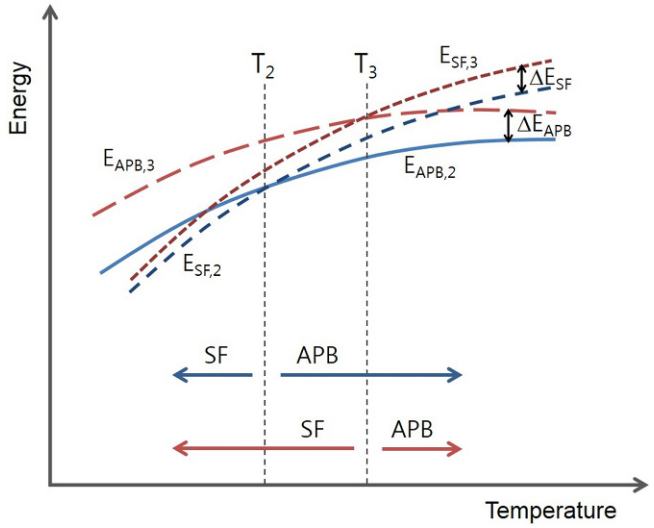

Fig. 9. Schematic diagram showing dislocation energies as functions of temperature.

ing temperature is more remarkable than the change of APBE with increasing temperature, which makes superdislocations coupled with APB cutting through the γ′ phase more dominant. At 982 °C, APB coupled pairs would be the favorable shearing mechanism, even in Alloy 3, which results in a decrease in the difference in creep properties between Alloy 2 and Alloy 3.

According to the creep results in the present study, the transition of the dominant γ′ cutting mechanism from dislocations coupled with SF to APB coupled pairs occurs with increasing temperature in both Alloy 2 and Alloy 3. However, the transition temperature is higher in Alloy 3 than in Alloy 2 owing to the difference in Ti contents.

The relationship between the energy of partial dislocations separated by SF in Alloy 2 and Alloy 3 can be considered as follows:

$$E_{SF,3}(T) - E_{SF,2}(T) = \Delta E_{SF}(T) \quad (1)$$

where $E_{SF,3}$(T) is the energy of partial dislocations coupled with SF as a function of temperature in Alloy 3, $E_{SF,2}(T)$ is that of Alloy 2, and $\Delta E_{SF}(T)$ is the difference of dislocation energy between two alloys due to different compositions. The energy of partial dislocations with APB can be considered in a similar way.

$$E_{APB,3}(T) - E_{APB,2}(T) = \Delta E_{APB}(T) \quad (2)$$

The extraction of equation (1) from equation (2) leads to following the equation (3).

$$E_{APB,3}(T) - E_{SF,3}(T) + E_{SF,2}(T) - E_{APB,2}(T) = \Delta E_{APB}(T) - \Delta E_{SF}(T) \quad (3)$$

Figure 9 is schematic diagram showing the variation of $E_{APB}(T)$ and $E_{SF}(T)$ as a function of temperature under the assumption that there is no maximum value within the creep temperature range. This assumption is reasonable because the maximum values of APBE and SFE are at much higher temperatures than the creep temperature range of the present study according to previous studies [14,21].

At the transition temperature of Alloy 2, T_2, $E_{SF,2}(T) = E_{APB,2}(T)$ but $E_{APB,3}(T) > E_{SF,3}(T)$ because at T_2, superdislocations coupled with SF is a favorable cutting mechanism in Alloy3. Therefore, from equation (3),

$$E_{APB,3}(T_2) - E_{SF,3}(T_2) + E_{SF,2}(T_2) - E_{APB,2}(T_2) = \Delta E_{APB}(T_2) - \Delta E_{SF}(T_2) > 0 \quad (4)$$

In similar way, an equation at T_3, the transition temperature of Alloy 3 can be derived,

$$E_{APB,3}(T_3) - E_{SF,3}(T_3) + E_{SF,2}(T_3) - E_{APB,2}(T_3) = \Delta E_{APB}(T_3) - \Delta E_{SF}(T_3) > 0 \quad (5)$$

because $E_{APB,3}(T_3) = E_{SF,3}(T_3)$ at T_3, but $E_{SF,2}(T_3) > E_{APB,2}(T_3)$.

Therefore, it can be rationalized that ΔE_{APB} is larger than ΔE_{SF} in the temperature range including T_2 and T_3. From the experimental results and simple calculations above, it is reasonable to consider that a higher amount of Ti in a single crystal superalloy increases APBE more significantly than SFE in the temperature range of the creep tests in this work.

4. CONCLUSION

The creep properties of the two experimental alloys were analyzed regarding the dislocation structures developed by creep deformation. The microstructure after creep tests, including the dislocation density, existence of SF, and formation of APB were found to be strongly dependent upon the amount of γ′ forming elements and the temperature.

(1) The addition of a certain amount of Ti in single crystal superalloy could improve resistance to the creep deformation at 900 °C and 950 °C owing to the dissociation of dislocations into partial dislocations with stacking faults.

(2) The two experimental alloys exhibited similar creep rupture lives and dislocation structures after creep at 982 °C.

(3) The transition of the γ′ cutting mechanism from dislocations coupled with SF to APB coupled pairs with increasing temperature appeared in the experimental alloys. However, the transition temperature is higher in Alloy 3 than in Alloy 2 owing to the difference in Ti contents.

(4) Ti increased APBE more significantly than SFE in the temperature range of creep tests in the present study.

ACKNOWLEDGEMENT

This study was supported financially by Fundamental Research Program of the Korean Institute of Materials Science (KIMS).

REFERENCES

1. J. H. Gu, C. H. Sung, J. H. Shin, S. M. Seo, and J. H. Lee, *Korean J. Met. Mater*. **54**, 261 (2016).
2. J. S. Lee, S. H. Kwon, B. G. Yoon, B. M. Chang, Y. G. Jung, and J. H. Lee, *Korean J. Met. Mater.* **54**, 838 (2016).
3. R. Hashizume, A. Yoshinari, T. Kiyono, Y. Murata, and M. Morinaga, *Superalloys 2004* (eds. K. A. Green, T. M. Pollock, H. Harada, T. E. Howson, R. C. Reed, J. J. Schirra, *et al.*), p. 53, TMS, Warrendale, USA (2000).
4. Y. Koizumi, T. Kobayashi, T. Yokogawa, J. Zhang, M. Osawa, M. Arai, *et al. Superalloys 2004* (eds. K. A. Green et al.), p. 35, TMS, Warrendale, USA (2000).
5. M. Zietara, S. Neumeier, M. Göken, and A. Czyrska-Filemonowicz, *Met. Mater. Int*. **23**, 126 (2017).
6. T. Kobayashi, Y. Koizumi, H. Harada, and T. Murakumo, *Acta Mater.* **52**, 3737 (2004).
7. J. X. Zhang, T. Murakumo, H. Harada, and Y. Koizumi, *Scripta Mater.* **48**, 287 (2003).
8. R. A. Hobbs, L. Zhang, C. M. F. Rae, S. Tin, A. K. Koul, and G. H. Gessinger, *Mat. Sci. Eng. A* **489**, 65 (2008).
9. C. Tian, G. Han, C. Cui, and X. Sun, *Mater. Design* **64**, 316 (2014).
10. J. H. Zhang, T. Jin, Y. B. Xu, Z. Q. Hu, and X. Wu, *J. Mater. Sci. Tech.* **18**, 159 (2002).
11. S. Ochiai, Y. Oya, and T. Suzuki, *Acta Metall. Mater.* **32**, 289 (1984).
12. G. N. Maniar and J. E. Bridge, Jr., *Metallography* **5**, 91 (1972).
13. Y. F. Wen, J. Sun, and J. Huang, *T. Nonferr. Metal. Soc.* **22**, 661 (2012).
14. H. P. Wang, M. Sluiter, and Y. Kawazoe, *Mater. T. JIM* **40**, 1301 (1999).
15. X. P. Tan, J. L. Liu, T. Jin, Z. Q. Hu, H. U. Hong, C. Y. Jo, *et al. Mat. Sci. Eng. A* **528**, 8381 (2011).
16. G. R. Leverant and B. H. Kear, *Metall. Mater. Trans. B* **1**, 491 (1970).
17. C. M. F. Rae, N. Matan, and R. C. Reed, *Mat. Sci. Eng. A* **300**, 125 (2001).
18. T. Link and M. Feller-Kniepmeier, *Metall. Mater. Trans. A* **23**, 99 (1992).
19. R. C. Reed, *The Superalloys*, pp.65-73, Cambridge University Press, Cambridge, UK (2006).
20. W. W. Milligan and S. D. Antolovich, *Metall. Mater. Trans. A* **22**, 2309 (1991).
21. L. Remy and A. Pineau, *Mater. Sci. Eng.* **36**, 47 (1978).
22. S. Tian, B. Qian, Y. Su, H. Yu, and X. Yu, *Mater. Sci. Forum* **706-709**, 2474 (2012).
23. T. Kruml, B. Viguier, J. Bonneville, and J. L. Martin, *Mat. Sci. Eng. A* **234-236**, 755 (1997).
24. J. S. Huo, J. T. Gou, L. Z. Zhou, X. Z. Qin, and G. S. Li, *J. Mater. Eng. Perform.* **16**, 55 (2007).
25. G. Bruno and H. C. Pinto, *Superalloys 2004* (eds. K. A. Green, T. M. Pollock, H. Harada, T. E. Howson, R. C. Reed, J. J. Schirra, *et al.*), p. 837, TMS, Warrendale, USA (2000).